

PARTICLE-BASED MULTISCALE MODELING OF INTRACELLULAR CALCIUM DYNAMICS*

ULRICH DOBRAMYS¹, STEN RÜDIGER², AND RADEK ERBAN¹

Abstract. Intracellular calcium is regulated by the release of Ca^{2+} ions from the endoplasmic reticulum via inisitol-4,5-triphosphate receptor channels. The resulting dynamics are highly diverse, lead to local calcium “puffs” as well as global waves propagating through cells. Local fluctuations in the number of calcium ions play a crucial role in the onset of these features. Previous modeling studies have focused on stochastic channel models coupled to deterministic diffusion of ions, thereby neglecting local fluctuations of the ion number. Tracking of individual ions is computationally difficult due to the scale separation in the Ca^{2+} concentration when channels are in the open or closed states. In this paper, a spatial multiscale model for investigating of the dynamics of puffs is presented. It couples Brownian motion (diffusion) of ions with a stochastic channel gating model. The model is used to analyze calcium puff statistics. Concentration time traces as well as channel state information are studied. We identify the regime in which puffs can be found and develop a mean-field theory to extract the boundary of this regime. Puffs are only possible when the time scale of channel inhibition is sufficiently large. Implications for the understanding of puff generation and termination are discussed.

Key words. Intracellular calcium, calcium puffs, multiscale modeling, stochastic diffusion

AMS subject classifications. 65C35, 92C42

1. Introduction. Intracellular calcium plays a major role in many signaling pathways, and regulates enzymatic activity and gene expression [7]. In order to control a variety of cell functions, cells orchestrate the local cytoplasmic calcium concentration via the release of Ca^{2+} ions through channels situated on the membrane of reservoirs, such as the endoplasmic and the sarcoplasmic reticulum. Modulation of the Ca^{2+} release regulates muscle contraction, pathway cross-talk and mitochondrial activity, and disruption of these processes is associated with various diseases such as early-onset Alzheimer’s [5, 43], heart failure [3, 2] as well as psychological conditions such as bipolar disorder and schizophrenia [6]. Hence, detailed knowledge about the underlying processes governing this signaling mechanism is required to allow progress in our understanding of these diseases.

In this paper, we focus on the release of calcium ions from the endoplasmic reticulum (ER) via inisitol-4,5-triphosphate receptor (IP_3R) channels. Upon binding of Ca^{2+} to binding sites on its cytosolic part, a channel opens and calcium ions flow from the ER into the cytoplasm. Channels occur in clusters of 10 to 20 channels. The opening of a single channel usually triggers the release of Ca^{2+} from other channels in the same cluster due to the increased Ca^{2+} concentration in their vicinity. This mechanism results in a highly localized increase of the cytosolic calcium concentration. These “puffs” of calcium ions have been detected and analyzed in experiments by using fluorescent calcium buffers [44, 22].

*Submitted to *Multiscale Modeling and Simulation* (May 28, 2022). The research leading to these results has received funding from the European Research Council under the *European Community’s Seventh Framework Programme (FP7/2007-2013)*/ ERC grant agreement n° 239870.

¹Mathematical Institute, University of Oxford, Radcliffe Observatory Quarter, Woodstock Road, Oxford, OX2 6GG, United Kingdom; e-mails: dobramysl@maths.ox.ac.uk; erban@maths.ox.ac.uk. Radek Erban would like to thank the Royal Society for a University Research Fellowship and the Leverhulme Trust for a Philip Leverhulme Prize.

²Institut für Physik, Humboldt-Universität zu Berlin, 12489 Berlin, Germany; e-mail: sten.ruediger@physik.hu-berlin.de. Sten Rüdiger acknowledges support from the Deutsche Forschungsgemeinschaft (RU1660 and IRTG 1740).

Traditional modeling approaches of intracellular calcium dynamics are based on deterministic macroscopic rate equations [25, 11], however the intrinsically random, erratic nature of calcium puffs [44] necessitates an approach going beyond the deterministic regime. Progress has been made by recognizing the importance of number fluctuations in the binding to the channels [37, 17] and using hybrid models, where the deterministic calcium concentration is coupled to stochastic channel binding models [34]. Recently, it was found that local fluctuations stemming from diffusive noise have a crucial influence in calcium dynamics, particularly in the inter-puff waiting time [21] but also on single-channel equilibrium behavior [42]. However, tracking the exact diffusion of individual ions in the complete computational domain is computationally intensive.

Here, for the first time, we apply spatial stochastic multiscale modeling to model full calcium dynamics and track individual ion positions in order to accurately incorporate diffusive noise. We take into account both activating and inhibitory channel properties. We study the dynamics of the calcium concentration as a function of the ion binding affinities and explore the regime where there exist puffs, as well as the regime in which channels do not close after their first opening. The paper is organized as follows: In the next Section 2 we discuss the spatial stochastic model for diffusion and channel gating used throughout this study. Section 3 discusses the multiscale approach we employ in order to reduce the computational effort required to track single ions and hence make this study feasible. In Section 4 we present results on the statistics of puffs extracted from simulated time series data, and study the transition between perpetually-open channel clusters and the parameter regime in which puffs can be observed. In addition, we develop a mean-field model for channel dynamics and use it to extract the boundary between the regimes. Finally, we summarize our findings in Section 5.

2. Spatial stochastic model for intracellular Ca^{2+} release. The spatial extent of our computational model consists of the three-dimensional domain Ω which models a part of the intracellular space. Ca^{2+} ions are able to undergo free diffusion in Ω . They bind to and dissociate from binding sites on the channels, which are positioned on a small area of the domain boundary, corresponding to the membrane of the ER. The domain geometry and boundary conditions are specified in Section 2.2. In the following sub-sections we discuss the components of this model in detail. The parameter values used throughout this study can be found in Table 1.

2.1. Diffusion - Brownian dynamics. A versatile method for the simulation of particles in a solution is given by Brownian Dynamics (BD). Collisions of particles with solution molecules lead to overdamped dynamics and random forcing on a sufficiently long time scale [14]. Assuming that there are $Q(t)$ free ions in the simulation domain at time t , the equation for Brownian motion of ions are given by

$$(2.1) \quad d\mathbf{X}_j = \sqrt{2D} d\mathbf{W}_j \quad j = 1, 2, \dots, Q(t),$$

where D is the diffusion coefficient of ions in solution, $\mathbf{X}_j(t) \in \Omega$ describes the trajectory of the j -th ion \mathbf{W}_j is a three-dimensional vector of independent Wiener processes. This approach dramatically reduces the dimensionality of the problem compared to molecular dynamics approaches wherein the degrees of freedom of every participating particle needs to be taken into account. Nevertheless, the computational load is still high compared to deterministic PDE-based approaches to diffusion. There are a number of approaches for simulating (2.1) in the literature, ranging from discretization with a fixed time step [4] to event-based methods [40, 29]. In this paper, we

Parameter description	Name	Value
Free Ca^{2+} diffusion constant[1]	D	$220 \mu\text{m}^2 \text{s}^{-1}$
Cytoplasmic Ca^{2+} concentration	c_0	$0.02 \mu\text{M}$
Edge length of computational domain	L	$5 \mu\text{m}$
Number of channels in cluster	C	9
Spacing between channels in cluster	ℓ	$0.15 \mu\text{m}$
Binding to activating site	a_a	$100 \mu\text{M}^{-1} \text{s}^{-1}$
Unbinding from activating site	b_a	20s^{-1}
Binding to inhibitory site	a_i	varies
Unbinding from inhibitory site	b_i	varies
Binding radius	ϱ	$0.03 \mu\text{m}$
Unbinding radius	σ	$0.015 \mu\text{m}$
Open channel current	I_C	0.1 pA
Edge length of BD regime	L_{BD}	$1 \mu\text{m}$
Compartment size	h	$0.2 \mu\text{m}$

TABLE 1

Parameter values for the spatial stochastic simulations, for physiologically relevant conditions [35].

discretize time with the time step Δt and use the Euler-Maruyama discretization of equation (2.1), i.e. the position of the j -th ion is updated according to

$$(2.2) \quad \mathbf{X}_j(t + \Delta t) = \mathbf{X}_j(t) + \sqrt{2D\Delta t} \boldsymbol{\xi}_j, \quad j = 1, 2, \dots, Q(t),$$

where $\boldsymbol{\xi}_j$ is a vector of three independent normally distributed random numbers with zero mean and unit variance.

2.2. Domain geometry and boundary conditions. In our simulations, the computational domain is given as cube $\Omega = [0, L]^3$ where the value of L is specified together with other parameters in Table 1. Ca^{2+} ions are able to undergo free diffusion in Ω which we simulate using (2.2). A cluster of nine IP_3R channels is positioned in a 3×3 grid with grid constant $\ell = 0.15 \mu\text{m}$, centered in the $z = 0$ plane, i.e. the positions of nine channels in the cluster are given as

$$(2.3) \quad \left[\frac{L}{2}, \frac{L}{2}, 0 \right], \quad \left[\frac{L}{2} \pm \ell, \frac{L}{2}, 0 \right], \quad \left[\frac{L}{2}, \frac{L}{2} \pm \ell, 0 \right], \quad \left[\frac{L}{2} \pm \ell, \frac{L}{2} \pm \ell, 0 \right].$$

Ions bind to and dissociate from binding sites on the channels. The boundaries of the computational domain at $x = 0$, $x = L$, $y = 0$, $y = L$, and $z = L$ are constant-concentration boundaries, hence they absorb and introduce ions, such that in the absence of open channels the concentration of Ca^{2+} in the computational domain is held at its equilibrium value, c_0 , on average. The boundary at $z = 0$ is reflective, corresponding to the membrane of the ER. Hence, ions can enter and leave the domain via the boundaries, in addition to being introduced through open channels.

If the channels are closed, then the average number of free ions in the computational domain, $\langle Q(t) \rangle$, is equal to $c_0|\Omega|$ where $|\Omega| = L^3$ is the volume of Ω . Using

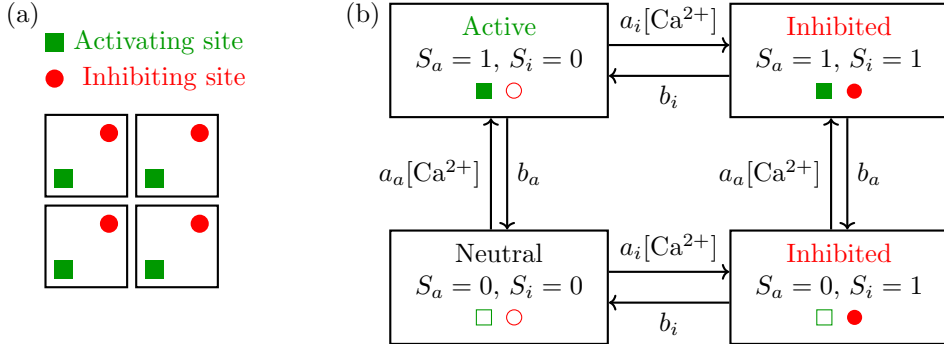
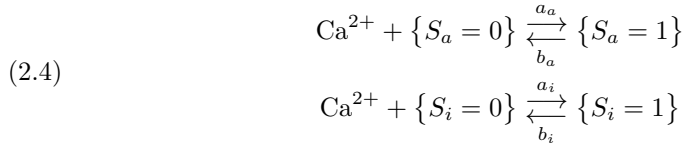


FIG. 1. (a) Sketch of a channel, containing 4 subunits with an activating ion binding site (green square) and an inhibiting site (red circle). (b) State space of a single subunit. Ions can bind to the activating and the inhibitory sites. A subunit is active only if it has an occupied activating site as well as an empty inhibiting site.

our parameter values (see Table 1), $c_0|\Omega| \approx 1.5 \times 10^3$. The average number of ions in the simulation domain, $\langle Q(t) \rangle$, increases when the channels are open (by around two orders of magnitude). In order to simulate the system over sufficiently long time intervals, we will use a multiscale approach, which we describe in detail in Section 3.

2.3. Stochastic channel binding model. The conformational changes between the open and closed states of IP₃R channels are controlled by the binding of Ca²⁺ to activating and inhibitory binding sites. These channels consist of 4 subunits, that can be itself in an active or a neutral/inhibited state. Each subunit has three different binding sites: An activating binding site for Ca²⁺ ions, an inhibitory binding site for Ca²⁺ ions, and an IP₃ binding site.

To accurately capture channel gating events, we employ a simplified DeYoung-Keizer model [11]. Here, we disregard IP₃ dynamics and consider the effects of IP₃ only via their influence on the dissociation constant b_i of Ca²⁺ ions from inhibitory binding sites. Free Ca²⁺ ions can bind to the activating and inhibitory sites, while bound ions can dissociate from occupied sites. Therefore, there are two reversible reactions in our model for each subunit of a channel:



The rates a_a and a_i describe the binding affinity of a Ca²⁺ ion to an activating and inhibitory binding site, respectively, while the off-rates b_a and b_i describe the corresponding dissociation reaction rates. The variables S_a and S_i describe the binding site state and can take values of 0 and 1. Channels consist of four subunits, with each subunit having one activating and one inhibitory Ca²⁺-binding site; see Figure 1. A model subunit can then be in three distinct states: neutral (no binding site occupied), active (only the activating site occupied) and inhibited (if the inhibitory site is occupied regardless of the state of the activating site). A channel then opens when at least three of its four subunits are in the active state.

2.4. Ion binding dynamics. In order to precisely capture channel opening and closing dynamics, we need to implement an accurate reversible BD binding model of

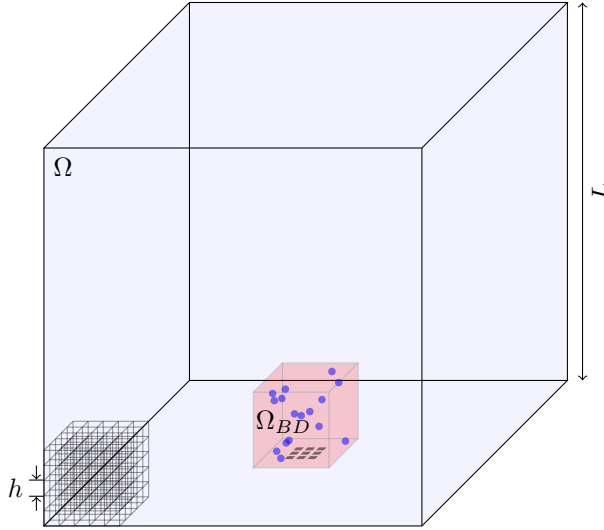


FIG. 2. Sketch of the computational domain Ω . It consists of two regions: The compartment-based part $\Omega \setminus \Omega_{BD}$ (with the compartment size h illustrated in the left bottom of the picture) and the BD domain Ω_{BD} (shown as a red box in the bottom center). The boundary in both x - and y -directions as well as the boundary at $z = L$ are constant-concentration boundaries, while the boundary at $z = 0$ is reflective. The channel cluster is positioned at the center of the $z = 0$ boundary (indicated as black squares), see (2.3).

Ca^{2+} ions to their corresponding binding sites. Ions become binding candidates as soon as they enter a half-sphere of radius ϱ around a binding site. They are then allowed to bind to the site with a probability P_λ per time step that they spend in the binding region [28, 15]. An ion bound to an activating site (resp. inhibitory site) is allowed to dissociate with a probability $1 - \exp(-b_a \Delta t)$ (resp. $1 - \exp(-b_i \Delta t)$) and placed at a distance of σ (unbinding radius) from the binding site. We use the values of binding and unbinding radii, ϱ and σ , as given in Table 1. Then we can pre-calculate the remaining parameter P_λ (binding probability) before the start of simulations using the approach described in [28, Section 5].

2.5. Channel opening and calcium flux. Each channel has four subunits. Let $S_a^{j,k}(t)$ (resp. $S_i^{j,k}(t)$), $j = 1, 2, \dots, 9$, $k = 1, 2, 3, 4$, be the state of the activating (resp. inhibiting) site of the k -th subunit of the j -th channel in the cluster. Then the number of active subunits of the j -th channel at time t is

$$N_a^j(t) = \sum_{k=1}^4 S_a^{j,k}(t) \left(1 - S_i^{j,k}(t)\right).$$

If $N_a^j(t) \geq 3$, then the channel is considered to be in an open state. When a channel is open, new ions are introduced with a rate of $3.12 \times 10^5 \text{ s}^{-1}$ (corresponding to channel current $I_C = 0.1 \text{ pA}$ [8, 36, 39]) at the channel site, simulating the flux of Ca^{2+} ions out of an active channel. The positions of released ions then evolve according to equation (2.2).

3. Multiscale approach. During a puff event, a large number of ions are released into the cytoplasm. If all channels are open, then one can estimate, for the parameter values given in Table 1, that our computational domain may contain of the

order of 10^5 ions during the peak of a puff. Since we are interested in time scales of minutes, tracking the individual position of this number of ions via Brownian dynamics becomes infeasible. However, high accuracy and individual ion positions are only needed in the vicinity of channel sites in order to ensure accurate implementation of BD binding dynamics, described in Section 2.4. Therefore, we split our computational domain into two regions: a cube

$$\Omega_{BD} = \left[\frac{L - L_{BD}}{2}, \frac{L + L_{BD}}{2} \right] \times \left[\frac{L - L_{BD}}{2}, \frac{L + L_{BD}}{2} \right] \times [0, L_{BD}]$$

containing the channel sites (red region in Figure 2), as well as the remaining space $\Omega \setminus \Omega_{BD}$ in which we will use a coarser description of ion movement as described in the next subsection. Here, $L_{BD} < L$ is the length of the edge of the cube Ω_{BD} . We use $L_{BD} = L/5$ in our simulations (see Table 1). In particular, we use BD simulations in a small fraction of $1/5^3 \approx 0.8\%$ of the computational domain Ω .

3.1. Compartment-based model for diffusion. We subdivide the region $\Omega \setminus \Omega_{BD}$ into compartments (cubes) with size h (illustrated in the bottom left of Figure 2) and employ a compartment-based method to simulate the movement of ions [16]. Ions are allowed to move between adjacent compartments with a rate of $d = D/h^2$. The compartment-based algorithm only stores and evolves the number of ions in each compartment (rather than following individual ions). An event-based stochastic simulation algorithm is used to efficiently simulate this system. Several equivalent methods have been developed in the literature, such as the Gillespie algorithm [24], the Gibson-Bruck Next Reaction method [23], the Next Subvolume method [13, 27], as well as Cao *et al.*'s Optimized Direct method [9].

In this paper, we employ the Gibson-Bruck Next Reaction method [23]. For each possible move between two neighboring compartments, a putative time for the next jump of an ion to occur is calculated. It is given by

$$(3.1) \quad t - \frac{\ln(r)}{d A_c(t)}$$

where $d = D/h^2$ is the jump rate per one ion, $A_c(t)$ is the current number of ions in the compartment from which an ion is jumping and r is a random number uniformly distributed in the interval $(0, 1)$. Clearly, the putative jump time (3.1) is infinity if $A_c(t) = 0$, i.e. if the corresponding compartment is empty. The putative times are smaller (on average) if the corresponding compartment contains more ions.

The putative jump times are inserted into a priority queue (a heap data structure [10]), which enables us to extract the earliest jump time and thus the next jump in logarithmic time. This move is then performed, and the numbers of ions in compartments (and the corresponding putative times and their entries in the priority queue) are updated. We then iterate this process by finding the minimal putative time and performing the corresponding ion jump at each iteration.

At the boundaries of the computational domain Ω (except for the boundary at $z = 0$, which is reflective), ions are absorbed (i.e. they leave the domain) or can enter with rates consistent with a constant equilibrium concentration of c_0 outside the domain. The jump rate from outside the domain into a compartment just inside the domain boundary is $c_0 D h$ which is used, instead of $d A_c(t)$, in (3.1) to compute the corresponding putative times.

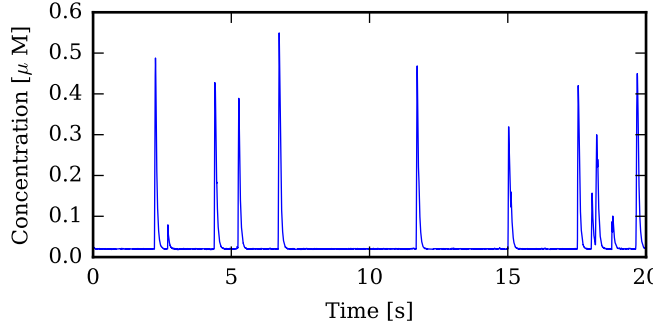


FIG. 3. Example concentration time trace for $a_i = 1 \mu\text{M}^{-1} \text{s}^{-1}$ and $b_i = 1 \text{s}^{-1}$.

3.2. Coupling the BD simulation in Ω_{BD} with the compartment-based approach in $\Omega \setminus \Omega_{BD}$. Several methods exist in order to couple the BD and compartment-based methods across their interface, such as the two-regime method (TRM) [18, 19] or the ghost-cell method [20]. Here, we employ the TRM. In order to accurately capture diffusion across the interface, the jump rates from adjacent compartments into Ω_{BD} need to be adjusted from $d = D/h^2$ to [18]

$$(3.2) \quad \frac{2D}{\sqrt{\pi h^2 D \Delta t}}.$$

These jump rates are used, instead of d , in (3.1) to compute the corresponding putative times. If the chosen move in the compartment regime is a jump from a compartment adjacent to the interface into Ω_{BD} , the occupancy number of the compartment is reduced by one and a new ion is added in Ω_{BD} at the distance x from the interface which is sampled from the probability distribution [18]

$$(3.3) \quad f(x) = \sqrt{\frac{\pi}{4D\Delta t}} \operatorname{erfc} \left[\frac{x}{4D\Delta t} \right],$$

where erfc is the complementary error function.

The rate (3.2) and the distribution (3.3) are used to transfer ions from $\Omega \setminus \Omega_{BD}$ into Ω_{BD} . In the opposite direction, the TRM transfers any ion from Ω_{BD} which during the time step interacts with the interface. For a detailed discussion and the derivation of the probabilities and jump rates above, please see references [18, 19, 20]. We employ the particle-based simulation library package *Tyche* which implements the TRM [30]. The TRM has also been recently implemented in Smoldyn [31].

4. Results. In the following section we present the results of our findings. Simulations were performed with the parameter values listed in Table 1 unless noted differently. In Section 4.1, we discuss Ca^{2+} puff statistics from simulation runs. We follow this by investigating the regimes in which puffs are visible in Section 4.2. A simple mean-field theory is then presented in Section 4.3. It describes the transition between puffs and perpetually open channels.

4.1. Puff statistics. Figure 3 displays a sample time trace of the Ca^{2+} concentration in the computational domain for $a_i = 1 \mu\text{M}^{-1} \text{s}^{-1}$ and $b_i = 1 \text{s}^{-1}$ for a time range of 20 s. The ion concentrations shows erratic calcium puffs with an amplitude of up to $0.5 \mu\text{M}$ on top of a constant background of $c_0 = 0.02 \mu\text{M}$. The puffs are

characterized by a sharp, almost instant increase in concentration, followed by an approximately exponential decay after the channel cluster closes. Puffs are separated by a refractory phase in which channel subunits are inhibited and the cluster cannot open.

We analyze the concentration data given as the time values t_j and concentration values c_j , $j = 1, 2, \dots, N$, (where N is the index of the last data point) by choosing a puff-starting threshold concentration value

$$(4.1) \quad c_t = \langle c_j \rangle + \sqrt{\text{Var}[c_j]},$$

i.e. one standard deviation above the mean concentration $\langle c_j \rangle$. The averaging in (4.1) is taken over all values of j , $j = 1, 2, \dots, N$, i.e. the sample mean and variance in (4.1) are estimated by

$$(4.2) \quad \langle c_j \rangle = \frac{1}{N} \sum_{j=1}^N c_j \quad \text{and} \quad \text{Var}[c_j] = \frac{1}{N-1} \sum_{j=1}^N (c_j - \langle c_j \rangle).$$

Puffs are identified by the concentration crossing the threshold point (4.1). Puff ending points are identified via a re-crossing of this value. The crossing points are given in the ordered index set

$$\mathcal{S} = \{j \mid c_{j-1} < c_t \text{ and } c_j \geq c_t, j = 2, 3, \dots, N-1\}$$

(puff starting indices) and

$$\mathcal{E} = \{j \mid c_j > c_t \text{ and } c_{j+1} \leq c_t, j = 2, 3, \dots, N-1\}$$

(puff ending indices). The sets \mathcal{S} and \mathcal{E} are enumerated by the puff index $1 \leq k \leq N_p$, where $N_p = |\mathcal{E}|$ is the number of finished puffs in the data set, i.e. we disregard the last index in \mathcal{S} if the last puff did not finish and denote

$$\mathcal{S} = \{s_1, s_2, \dots, s_{N_p}\} \quad \mathcal{E} = \{e_1, e_2, \dots, e_{N_p}\},$$

where the elements in \mathcal{S} (resp. \mathcal{E}) are ordered, i.e. $s_1 < s_2 < \dots < s_{N_p}$ (resp. $e_1 < e_2 < \dots < e_{N_p}$). The inter-puff times are then given by

$$(4.3) \quad \mathcal{T} = \left\{ t_{s_{k+1}} - t_{e_k} \mid s_{k+1} \in \mathcal{S}, e_k \in \mathcal{E}, 1 \leq k \leq N_p - 1 \right\} \cap (t_p, \infty),$$

where the threshold $t_p = 0.25$ s. This threshold filtering decreases the number of puffs considered by removing the puffs which are not well separated. The distribution of inter-puff times (histogram of set \mathcal{T}) is shown in Figure 4 for a set of 545 puff intervals. Its shape is similar to a Gamma distribution

$$(4.4) \quad p(\tau) = \frac{1}{\Gamma(\kappa)\theta^\kappa} x^{\kappa-1} e^{-\tau/\theta}.$$

Indeed, when choosing $\kappa = 4.08$ and $\theta = 0.81$ s in equation (4.4) (such that the resulting distribution has the same mean and variance as our data), the comparison is good. As the Erlang distribution (the special case of a Gamma distribution with $\kappa \in \mathbb{N}$) results from summing κ exponentially-distributed random variables, we can speculate that an effective model of calcium channel opening might be described

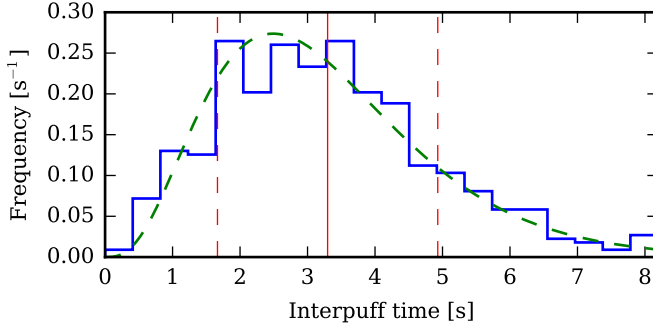


FIG. 4. *Inter-puff time distribution for a set of $N_p = 1151$ puffs (resulting in 545 puff intervals after threshold filtering (4.3)) from simulations with a total duration of 3 simulation hours. The mean inter-puff time is 3.30 ± 1.63 s (indicated by the red vertical lines). The green dashed line displays Gamma distribution (4.4) with $\kappa = 4.08$ and $\theta = 0.81$ s.*

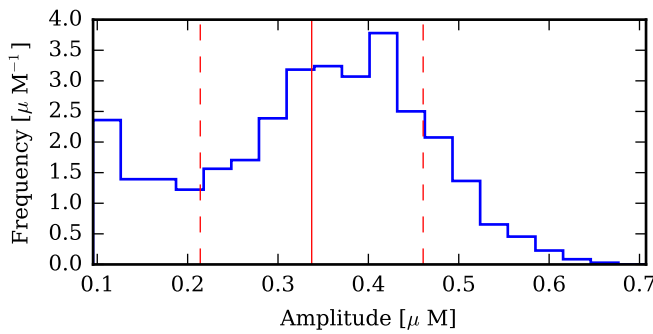


FIG. 5. *Amplitude distribution for a set of $N_p = 1151$ puffs from simulations with a total duration of 3 simulation hours. The mean puff amplitude is $0.34 \pm 0.12 \mu\text{M}$ (indicated by the red vertical lines).*

by a four-stage binding/unbinding process. The maximum in the inter-puff time distribution, $\tau_m \approx 2.7$ s can be interpreted as the typical time between puffs in this system.

The distribution of puff amplitudes are determined by taking the maximum value in a previously-determined puff interval

$$\mathcal{A} = \left\{ a_k \mid a_k = \max_{s_k \leq j \leq e_k} c_j, \text{ where } s_k \in \mathcal{S}, e_k \in \mathcal{E}, 1 \leq k \leq N_p \right\}.$$

The amplitude distribution (histogram of set \mathcal{A}) is shown in Figure 5 and mirrors the broad distribution characterized in experiments [12].

The puff durations are calculated by considering the full duration at half maximum [12]. To this end, we calculate the indices of crossings of the half maximum threshold on the rising slope of a puff

$$\mathcal{R} = \left\{ r_k \mid r_k = \max\{j \mid c_{j-1} < a_k/2 \text{ and } c_j \geq a_k/2 \text{ and } s_k \leq j \leq e_k\}, \text{ where } s_k \in \mathcal{S}, e_k \in \mathcal{E}, a_k \in \mathcal{A}, 1 \leq k \leq N_p \right\},$$

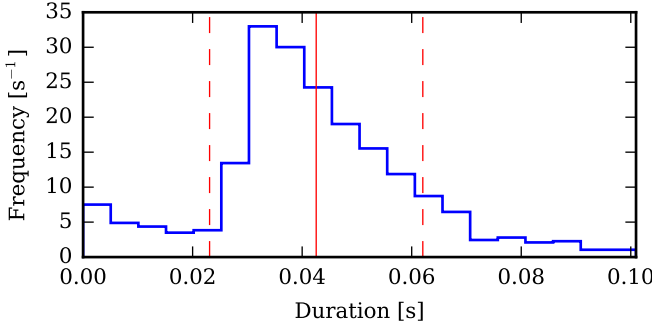


FIG. 6. Puff duration (full duration at half amplitude) distribution for a set of $N_p = 1151$ puffs from simulations with a total duration of 3 simulation hours. The mean puff duration is 0.04 ± 0.02 s (indicated by the red vertical lines).

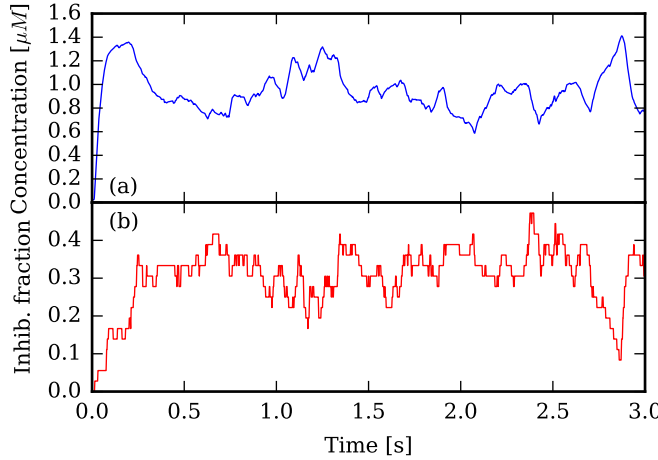


FIG. 7. (a) Calcium concentration as a function of time for $a_i = 0.1 \mu\text{M}^{-1} \text{s}^{-1}$ and $b_i = 5 \text{s}^{-1}$. Other parameter values are given in Table 1. (b) Fraction of inhibited channel subunits as a function of time. Note that the channel cluster stays perpetually active in this configuration.

and the falling slope of a puff

$$\mathcal{F} = \left\{ f_k \mid f_k = \min\{j \mid c_j > a_k/2 \text{ and } c_{j+1} \leq a_k/2 \text{ and } s_k \leq j \leq e_k\}, \text{ where } s_k \in \mathcal{S}, e_k \in \mathcal{E}, a_k \in \mathcal{A}, 1 \leq k \leq N_p \right\}.$$

The puff durations are then calculated via

$$\mathcal{D} = \{t_{f_k} - t_{r_k} \mid f_k \in \mathcal{F}, r_k \in \mathcal{R}, 1 \leq k \leq N_p\}.$$

The distribution of puff durations (histogram of set \mathcal{D}) is plotted in Figure 6. The distribution is sharply peaked around 0.03 s and has a long tail stemming from repeated cluster re-openings during the concentration decay phase. The mean puff lifetime is within the range 40–70 ms measured in experiments [12].

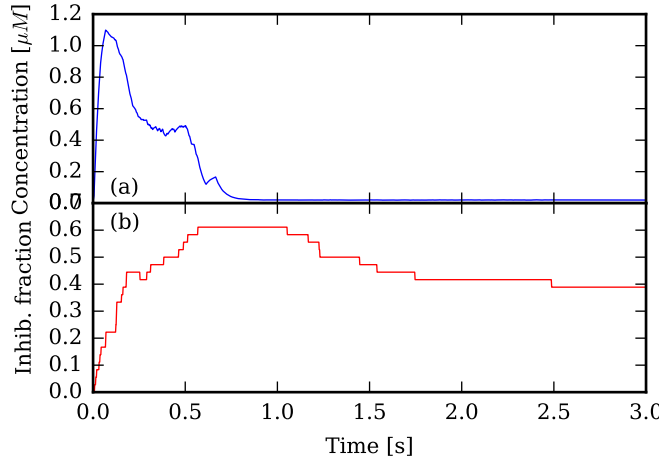


FIG. 8. (a) The Ca^{2+} concentration as a function of time for the inhibitory site binding parameters $a_i = 0.1 \mu\text{M}^{-1} \text{s}^{-1}$ and $b_i = 0.1 \text{s}^{-1}$. Other parameter values are given in Table 1. (b) The fraction of occupied inhibitory binding sites in the channel cluster as a function of time. Note that the time scale of inhibition decay is long enough for the calcium concentration to decay completely, thus the channel cluster closes and we can identify well-defined puffs.

4.2. Inhibition transition. Figures 7 and 8 show the results of a simulation run with two different values of inhibitory site dissociation rate b_i , illustrating two different modes of behavior. We use the same value of a_i in both figures (the rest of parameter values are given in Table 1). Figure 7 shows the results of a simulation run with $b_i = 5 \text{s}^{-1}$ (corresponding to a dissociation constant of $K_D = b_i/a_i = 50 \mu\text{M}$). These simulation parameters are consistent with the modeling of calcium puffs in the literature and used in hybrid PDE-based models [35]. Figure 7(a) shows the Ca^{2+} concentration in the computational domain Ω , while Figure 7(b) displays the fraction of occupied inhibitory sites in the channel cluster as a function of time. Due to the large dissociation rate, the necessary level of bound inhibitory sites can never be sustained long enough for all the channels in the cluster to close at the same time. Therefore, the Ca^{2+} concentration is kept at a level where empty activating sites are immediately filled and the channel cluster stays perpetually open. Hence, puff termination in this case can be speculated to be facilitated by a mechanism other than channel inhibition, such as ER Ca^{2+} reservoir depletion or a mechanism involving dissociation of IP_3 [32]. We checked the influence of lowering the binding radius ϱ to 6 nm and found that it had no effect on the channel cluster closing.

In contrast, a lower inhibitory site dissociation constant yields well-defined calcium puffs in our particle-based simulation scheme. Figure 8 displays data from simulation runs with $b_i = 0.1 \text{s}^{-1}$ (which corresponds to $K_D = b_i/a_i = 1 \mu\text{M}$). Here, inhibitory sites binding is sustained on a high level for a long enough time such that all channels close and the excess Ca^{2+} is removed. Hence there are time intervals when the cluster concentration decreases and reaches the equilibrium Ca^{2+} concentration c_0 . Puffs are therefore clearly delineated and separated with a well-defined inter-puff time.

Hence there exist two regimes: a puff regime (Figure 8) and a regime with perpetually open channel clusters (Figure 7). We now proceed to characterize concentration

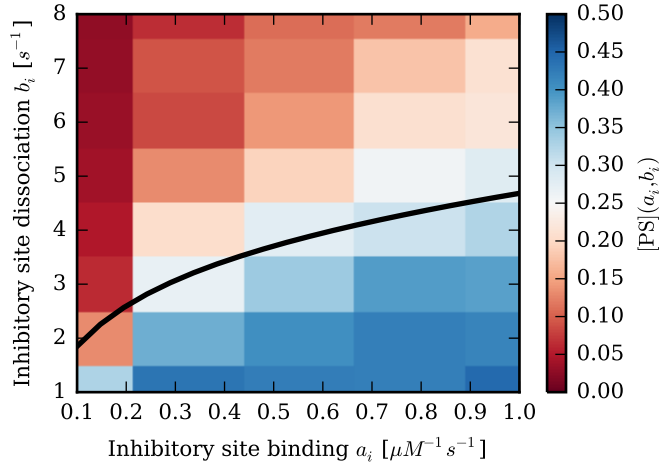


FIG. 9. Phase plot of a_i and b_i . Color indicates the puff score (4.5) for the given set of parameters listed in Table 1. The black line shows the numerically-determined phase boundary from the mean-field model (4.6)–(4.8).

and open channel time traces to find under which conditions well-defined puffs are possible. To this end, we use the “puff score” characterization function introduced in [26], which quantifies the spike-ness of a given time trace of the number of open channels. We denote the number of open channels at time point t_j by O_j , $j = 1, 2, \dots, N$, i.e. $O_j \in \{0, 1, 2, \dots, C\}$ where $C = 9$ in our simulations. Then the puff score is defined by

$$(4.5) \quad [\text{PS}](a_i, b_i) = \frac{1}{C} \frac{\text{Var}[O_j]}{\langle O_j \rangle}.$$

where the averages are again take over all values of j , $j = 1, 2, \dots, N$ (compare with (4.2)). The puff score (4.5) can take values in $[0, 0.5]$. A puff score greater than 0.25 indicates channel excitability and therefore the existence of puffs in the system.

In order to visualize the two parameter regimes, we performed simulations for different inhibitory site binding parameters $a_i \in [0.1, 1] \mu\text{M}^{-1} \text{s}^{-1}$ and $b_i \in [1, 10] \text{s}^{-1}$ for a simulation time duration of 100 s. We extracted the number of open channels over time and calculated the puff score (4.5). Figure 9 displays this quantity. The color indicates the value of $[\text{PS}](a_i, b_i)$. The transition between the two regimes is not sharp, but gradual, especially for higher a_i . This is due to prolonged channel reopenings becoming more likely due to faster dissociation of bound inhibiting ions when b_i approaches the transition. The phase boundary is consistent with a dissociation constant of $4 \mu\text{M} < K_D < 10 \mu\text{M}$.

In order to study the influence of the diffusion constant on the boundaries of the puff regime, we performed a similar set of simulations with a lower Ca^{2+} diffusion constant of $D = 20 \mu\text{m}^2 \text{s}^{-1}$. The result is shown in Figure 10. With a lower diffusion constant, the calcium concentration in the channel cluster nanodomains decays more slowly. For puffs to exist, the time scale of the decay of inhibitory site binding needs to be longer than the time scale of Ca^{2+} decay. Hence, the boundary separating the two regimes is pushed to smaller values of the inhibitory dissociation rate b_i , corresponding to approximately $1 \mu\text{M} < K_D < 2 \mu\text{M}$. Hence, the effective diffusion constant plays

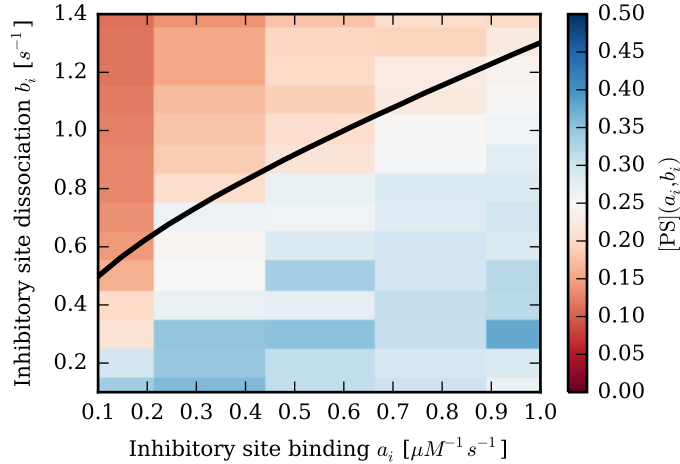


FIG. 10. Phase plot of a_i and b_i with a low diffusion constant $D = 20 \mu\text{m}^2 \text{s}^{-1}$. The other parameters are given in Table 1. Color indicates the puff score (4.5). The black line shows the numerically-determined phase boundary from the mean-field model (4.6)–(4.8).

an important role in determining the boundary between the two regimes. Note, that the overall variation of the puff score $[\text{PS}](a_i, b_i)$ is smaller compared to the case of $D = 220 \mu\text{m}^2 \text{s}^{-1}$, therefore Ca^{2+} puffs become less pronounced with slower ion diffusion.

4.3. Mean-field model. In order to find an approximate phase diagram to determine the parameter regimes in which calcium puffs occur, we developed a simplified non-spatial model. To this end, we consider an ensemble of identical channels that interact by a shared calcium domain (all-to-all coupling). The concentration $c(t)$ in the $1 \mu\text{m}^3$ cube around a channel undergoes exponential decay with a phenomenological decay parameter λ due to diffusive equilibration, and a linear increase with an ion influx rate ν when the channel is open. The open states of the ensemble of channels is determined by the mean number of occupied activating and inhibitory binding sites per channel, $a(t)$ and $b(t)$, in a similar way as in the spatial model above. In a simple representation of the subunit dynamics and their binding cooperativity we require that a channel is open at a given time t if $a(t) \geq 3$ and $b(t) < 2$. Here the variables $a(t)$ and $b(t)$ describe how many subunits, on average, have activating and inhibitory ions bound to their respective binding sites. They evolve according to the mass-action rate equations corresponding to the reactions (2.4). Hence the model equations are:

$$(4.6) \quad \frac{\partial c}{\partial t} = \Theta(a - 3) \Theta(2 - b) \nu - \lambda (c - c_0) ,$$

$$(4.7) \quad \frac{\partial a}{\partial t} = a_a c (4 - a) - b_a a ,$$

$$(4.8) \quad \frac{\partial b}{\partial t} = a_i c (4 - b) - b_i b .$$

c_0	0.02 μM	Background Ca^{2+}
ν	$5.18 \times 10^2 \mu\text{M s}^{-1}$	Source rate
λ	22.9 s^{-1} ($D = 220 \mu\text{m}^2 \text{ s}^{-1}$) 2.2 s^{-1} ($D = 20 \mu\text{m}^2 \text{ s}^{-1}$)	Ca^{2+} decay
a_a	$100 \mu\text{M}^{-1} \text{ s}^{-1}$	Activating site binding
b_a	20 s^{-1}	Activating site unbinding
a_i	$[0.1, 1] \mu\text{M}^{-1} \text{ s}^{-1}$	Inhibiting site binding
b_i	$[0.1, 0.8] \text{ s}^{-1}$	Inhibiting site unbinding

TABLE 2
Parameter values for the ODE mean-field model (4.6)-(4.8).

Here, $\Theta(x)$ is the Heaviside function with the properties

$$\Theta(x) = \begin{cases} 0 & \text{for } x < 0 \\ 1/2 & \text{for } x = 0 \\ 1 & \text{for } x > 0 \end{cases}.$$

The first term on the right hand side of equation (4.6) describes the above-mentioned channel openings: The channels only open if three subunits are active and not inhibited. The influx rate is determined via the channel current $\nu = (2eV)^{-1}I_C = 518.28 \mu\text{M}$ (where $e = 1.602 \times 10^{-19} \text{ C}$ is the electron charge; the in-flowing ions are assumed to be spread over a volume of $V = 1 \mu\text{m}^3$). This value is also consistent with influx rates extracted from the rising flanks of puffs in our simulations. The exponential decay parameter λ was determined by fitting an exponential decay to calcium puff simulation data. The parameters of the mean-field model are summarized in Table 2.

Figure 11 shows data from three representative numerical solutions of the ODE system (4.6)-(4.8) where the inhibitory binding rate is set to $a_i = 0.5 \mu\text{M}^{-1} \text{ s}^{-1}$. The initial conditions are $c(0) = c_0$, $a(0) = 4$ and $b(0) = 0$. The concentration $c(t)$ in Figure 11(a) shows a puff with its characteristic exponential decay to c_0 . For $b_i = 2 \text{ s}^{-1}$, $c(t)$ returns to its equilibrium value c_0 , while for higher values, it oscillates at a high concentration level. These two states correspond to the “puff” regime and the “always open” regime, respectively. Figure 11(b) shows the corresponding trajectories in $a(t)$ - $b(t)$ space. When the trajectory, after its initial transient phase, does not touch the line segment $\{(a, 2) \text{ for } a \in (3, 4)\}$, highlighted in gray in Figure 11(b), the concentration will decay to c_0 and the system returns to its original state. If, however the $a(t)$ - $b(t)$ trajectory hits this boundary, the system stays excited and the channels stay perpetually open.

We now proceed to find the mean-field phase boundary between the “puff” regime and the “perpetually-open” regime. To numerically test if a given parameter set a_i , b_i falls into one of the two regimes, we first let the system evolve until it reaches a steady state. We then identify the regime the system is in. A bisection algorithm is then used to find the boundary $b_i(a_i)$ between the two regimes. The black lines in Figures 9 and 10 show the extracted phase boundaries for the parameter values given in Table 2.

5. Conclusions. In this paper, we have reported a novel application of a particle-based spatial algorithm for diffusion to investigate the influence of diffusive noise on

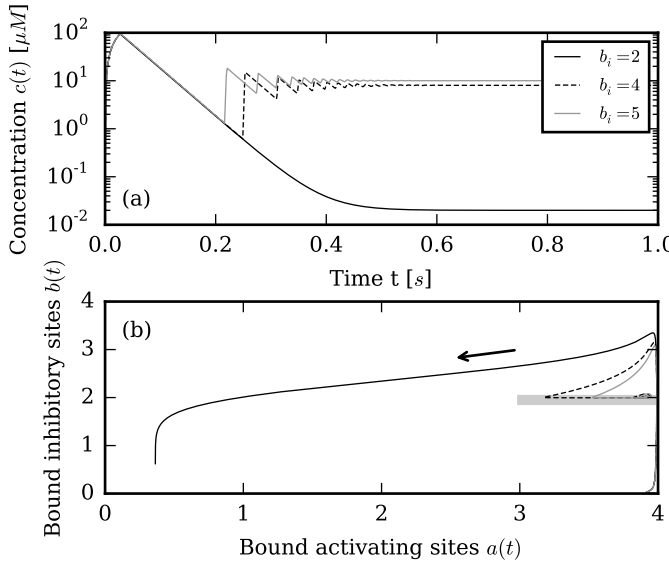


FIG. 11. (a) Concentration over time and (b) phase space trajectories of the mean field system (4.6)-(4.8). The ratchet-like oscillation visible in the concentration traces for $b_i = 4 \text{ s}^{-1}$ and 5 s^{-1} stems from the channels being re-activated repeatedly due to insufficient inhibition.

the dynamics of intracellular calcium release. Particle number noise in calcium micro-domains has attracted interest in recent studies [21, 41, 42] and it is important to clarify whether calcium diffusion as an additional noise source needs to be incorporated to obtain a better understanding of sub-cellular calcium signals.

In order to make this study feasible, we split the domain into a compartment-based regime and a Brownian dynamics regime, coupled via the TRM. This allowed us to model the dynamics of full puffs, including release of a realistic number of ions and inhibition dynamics. We extracted concentration time traces and analyzed the resulting puff statistics. The inter-puff time distribution as well as the distributions of puff amplitudes and lifetimes agree qualitatively with experimental data in the literature. Our simulations are thus not only important examples for the usefulness of the two-regime method but are also relevant for the understanding of physiological properties of calcium signals.

We then proceeded to analyze the binding parameter regimes under which well-defined Ca^{2+} puffs are possible. We found that, surprisingly, an inhibitory binding site dissociation constant $K_D = 50 \mu\text{M}$ consistent with the literature and patch-clamp experiments, does not yield puffs in our model. In this parameter regime, channels stay perpetually open. In order to investigate the transition between well-defined puffs and perpetually-open channels, we characterized calcium concentration traces for various combinations of the inhibitory site binding parameters. The phase boundary visible in our data is consistent with a dissociation constant in the region $4 \mu\text{M} < K_D < 10 \mu\text{M}$. Lower values of the Ca^{2+} diffusion constant yield a phase boundary at smaller inhibitory site dissociation rates and thus an even smaller dissociation constant. Given the reliable puff generation and termination in previous studies based on fitted gating models with large K_D [35, 38] this is an unexpected result.

Why does our model not show the same robust termination as the hybrid ap-

proaches? In the latter models the binding and unbinding to the receptors is stochastic but the calcium distribution is calculated from deterministic reaction-diffusion equations. There are two possibilities for the weak puff termination: First, in the TRM simulations at large K_D there could be insufficient inhibition to the channels during the early phase of a puff. This means that no or perhaps only one subunit per channel binds inhibitory calcium, while reliable inhibition requires binding of three or four calcium ions. In a hybrid approach, a deep inhibitory state is presumably achieved owing to the large local nano-domain around each open channel displayed in the solution of deterministic calcium equations [33]. Here, a channel is not inhibited by the shared calcium in the domain but by its own released calcium (self-inhibition). A second possibility is that there could be re-activations of closed channels during the falling phase of the puff after the channels have lost the inhibiting calcium. In this scenario, the decrease of residual calcium within the domain is slower than the de-inhibition process.

A hint on the origin of weak puff termination is given by the final analysis of our study. We developed a mean-field ODE model that captures the average binding state of the cluster's activating and inhibitory sites as well as the resulting Ca^{2+} concentration in a shared and well-mixed micro-domain. This model displays a sharp phase boundary between the two regimes, which agrees well with the data from our spatial simulations. This agreement suggests the second scenario, i.e., that the inhibitory binding decays fast and channels become re-activated by residual calcium in the cluster vicinity. In fact, Figure 11(b) indicates that if the inhibition $b(t)$ decays faster than a certain threshold, channels become active again. However, it is also likely, that diffusive noise mixes calcium in the cluster domain and diminishes the localized domains around open channels. Evidence for an inhomogeneous or homogeneous calcium distribution in the cluster is hard to obtain from our simulations because of the short lifetime of nano domains. In any case, our study highlights the role of the local calcium concentration in the termination of puffs and shows that puffs are very sensitive to fluctuations of residual calcium remaining after channel closing. It has to be noted though, that, apart from the diffusive noise, there are other differences of the current BD setup and the former hybrid approaches. Notably, these include the presence of calcium-binding buffers and the action of SERCA pump terms on the ER membrane boundary and it remains to be analyzed to which extent these differences affect puff termination.

REFERENCES

- [1] N. L. ALLBRITTON, T. MEYER, AND L. STRYER, *Range of messenger action of calcium ion and inositol 1,4,5-trisphosphate.*, Science (New York, N.Y.), 258 (1992), pp. 1812–1815.
- [2] M. E. ANDERSON, *Three Ways to Die Suddenly: Do They All Require Calcium Calmodulin-Dependent Protein Kinase II?*, Transactions of the American Clinical and Climatological Association, 125 (2014), pp. 173–85.
- [3] M. E. ANDERSON, J. H. BROWN, AND D. M. BERS, *CaMKII in myocardial hypertrophy and heart failure.*, Journal of molecular and cellular cardiology, 51 (2011), pp. 468–73.
- [4] S. ANDREWS AND D. BRAY, *Stochastic simulation of chemical reactions with spatial resolution and single molecule detail*, Physical Biology, 1 (2004), pp. 137–151.
- [5] M. J. BERRIDGE, *Calcium signalling and Alzheimer's disease.*, Neurochemical research, 36 (2011), pp. 1149–56.
- [6] M. J. BERRIDGE, *Calcium signalling and psychiatric disease: bipolar disorder and schizophrenia.*, Cell and tissue research, 357 (2014), pp. 477–92.
- [7] M. J. BERRIDGE, P. LIPP, AND M. D. BOOTMAN, *The versatility and universality of calcium signalling.*, Nature reviews. Molecular cell biology, 1 (2000), pp. 11–21.

[8] L. BRUNO, G. SOLOVEY, A. C. VENTURA, S. DARGAN, AND S. P. DAWSON, *Quantifying calcium fluxes underlying calcium puffs in Xenopus laevis oocytes*, Cell Calcium, 47 (2010), pp. 273–286.

[9] Y. CAO, H. LI, AND L. PETZOLD, *Efficient formulation of the stochastic simulation algorithm for chemically reacting systems.*, The Journal of chemical physics, 121 (2004), pp. 4059–67.

[10] T. H. CORMEN, C. E. LEISERSON, R. L. RIVEST, AND C. STEIN, *Introduction to Algorithms*, The MIT Press, Cambridge, MA, 3rd ed., 2009.

[11] G. W. DE YOUNG AND J. KEIZER, *A single-pool inositol 1,4,5-trisphosphate-receptor-based model for agonist-stimulated oscillations in Ca²⁺ concentration.*, Proceedings of the National Academy of Sciences, 89 (1992), pp. 9895–9899.

[12] G. D. DICKINSON AND I. PARKER, *Factors determining the recruitment of inositol trisphosphate receptor channels during calcium puffs*, Biophysical Journal, 105 (2013), pp. 2474–2484.

[13] J. ELF AND M. EHRENBERG, *Spontaneous separation of bi-stable biochemical systems into spatial domains of opposite phases*, Systems Biology, 1 (2004), pp. 230–236.

[14] R. ERBAN, *From molecular dynamics to Brownian dynamics*, Proceedings of the Royal Society A, 470 (2014), p. 20140036.

[15] R. ERBAN AND S. J. CHAPMAN, *Stochastic modelling of reaction-diffusion processes: algorithms for bimolecular reactions.*, Physical biology, 6 (2009), p. 046001.

[16] R. ERBAN, S. J. CHAPMAN, AND P. MAINI, *A practical guide to stochastic simulations of reaction-diffusion processes*, 35 pages, available as <http://arxiv.org/abs/0704.1908>, 2007.

[17] M. FALCKE, *On the role of stochastic channel behavior in intracellular Ca²⁺ dynamics*, Biophysical journal, 84 (2003), pp. 42–56.

[18] M. B. FLEGG, S. J. CHAPMAN, AND R. ERBAN, *The two-regime method for optimizing stochastic reaction-diffusion simulations.*, Journal of the Royal Society, Interface / the Royal Society, 9 (2012), pp. 859–68.

[19] M. B. FLEGG, S. J. CHAPMAN, L. ZHENG, AND R. ERBAN, *Analysis of the Two-Regime Method on Square Meshes*, SIAM Journal on Scientific Computing, 36 (2014), pp. B561–B588.

[20] M. B. FLEGG, S. HELLANDER, AND R. ERBAN, *Convergence of methods for coupling of microscopic and mesoscopic reaction-diffusion simulations*, Journal of Computational Physics, (2015).

[21] M. B. FLEGG, S. RÜDIGER, AND R. ERBAN, *Diffusive spatio-temporal noise in a first-passage time model for intracellular calcium release.*, The Journal of chemical physics, 138 (2013), p. 154103.

[22] D. FRAIMAN, B. PANDO, S. DARGAN, I. PARKER, AND S. P. DAWSON, *Analysis of puff dynamics in oocytes: interdependence of puff amplitude and interpuff interval.*, Biophysical journal, 90 (2006), pp. 3897–3907.

[23] M. A. GIBSON AND J. BRUCK, *Efficient Exact Stochastic Simulation of Chemical Systems with Many Species and Many Channels*, The Journal of Physical Chemistry A, 104 (2000), pp. 1876–1889.

[24] D. T. GILLESPIE, *A general method for numerically simulating the stochastic time evolution of coupled chemical reactions*, Journal of Computational Physics, 22 (1976), pp. 403–434.

[25] A. GOLDBETER, G. DUPONT, AND M. J. BERRIDGE, *Minimal model for signal-induced Ca²⁺ oscillations and for their frequency encoding through protein phosphorylation.*, Proceedings of the National Academy of Sciences of the United States of America, 87 (1990), pp. 1461–1465.

[26] Y. HAO, P. KEMPER, AND G. D. SMITH, *Reduction of calcium release site models via fast/slow analysis and iterative aggregation/disaggregation*, Chaos, 19 (2009), pp. 1–13.

[27] J. HATTNE, D. FANGE, AND J. ELF, *Stochastic reaction-diffusion simulation with MesoRD.*, Bioinformatics (Oxford, England), 21 (2005), pp. 2923–4.

[28] J. LIPKOVÁ, K. C. ZYGALAKIS, S. J. CHAPMAN, AND R. ERBAN, *Analysis of Brownian Dynamics Simulations of Reversible Bimolecular Reactions*, SIAM Journal on Applied Mathematics, 71 (2011), pp. 714–730.

[29] T. OPPLESTRUP, V. BULATOV, A. DONEV, M. KALOS, G. GILMER, AND B. SADIGH, *First-passage kinetic Monte Carlo method*, Physical Review E, 80 (2009), p. 066701.

[30] M. ROBINSON, *Tyche Stochastic Simulation Package*. <http://tycheSSA.github.com>.

[31] M. ROBINSON, S. ANDREWS, AND R. ERBAN, *Multiscale reaction-diffusion simulations with Smoldyn*. to appear in Bioinformatics, doi: 10.1093/bioinformatics/btv149, 2015.

[32] S. RÜDIGER, P. JUNG, AND J.-W. SHUAI, *Termination of ca²⁺ release for clustered ip₃r channels*, PLoS computational biology, 8 (2012), p. e1002485.

[33] S. RÜDIGER, C. NAGAIAH, G. WARNECKE, AND J. SHUAI, *Calcium domains around single and clustered ip₃ receptors and their modulation by buffers*, Biophysical journal, 99 (2010), pp. 3–12.

- [34] S. RÜDIGER, J. SHUAI, W. HUISINGA, C. NAGAIAH, G. WARNECKE, I. PARKER, AND M. FALCKE, *Hybrid stochastic and deterministic simulations of calcium blips*, Biophysical journal, 93 (2007), pp. 1847–1857.
- [35] S. RÜDIGER, J. W. SHUAI, AND I. M. SOKOLOV, *Law of mass action, detailed balance, and the modeling of calcium puffs*, Physical Review Letters, 105 (2010).
- [36] I. F. SMITH AND I. PARKER, *Imaging the quantal substructure of single IP3R channel activity during Ca2+ puffs in intact mammalian cells.*, Proceedings of the National Academy of Sciences of the United States of America, 106 (2009), pp. 6404–6409.
- [37] S. SWILLENS, G. DUPONT, L. COMBETTES, AND P. CHAMPEIL, *From calcium blips to calcium puffs: theoretical analysis of the requirements for interchannel communication.*, Proceedings of the National Academy of Sciences of the United States of America, 96 (1999), pp. 13750–13755.
- [38] G. ULLAH, I. PARKER, D.-O. D. MAK, AND J. E. PEARSON, *Multi-scale data-driven modeling and observation of calcium puffs*, Cell calcium, 52 (2012), pp. 152–160.
- [39] H. VAIS, J. K. FOSKETT, AND D.-O. DANIEL MAK, *Unitary Ca(2+) current through recombinant type 3 InsP(3) receptor channels under physiological ionic conditions.*, The Journal of general physiology, 136 (2010), pp. 687–700.
- [40] J. VAN ZON AND P. TEN WOLDE, *Green's-function reaction dynamics: a particle-based approach for simulating biochemical networks in time and space*, Journal of Chemical Physics, 123 (2005), p. 234910.
- [41] S. H. WEINBERG AND G. D. SMITH, *The influence of ca 2+ buffers on free [ca 2+] fluctuations and the effective volume of ca 2+ microdomains*, Biophysical journal, 106 (2014), pp. 2693–2709.
- [42] N. WIEDER, R. FINK, AND F. VON WEGNER, *Exact stochastic simulation of a calcium microdomain reveals the impact of ca 2+ fluctuations on ip 3 r gating*, Biophysical journal, 108 (2015), pp. 557–567.
- [43] N. K. WOODS AND J. PADMANABHAN, *Neuronal calcium signaling and Alzheimer's disease.*, Advances in experimental medicine and biology, 740 (2012), pp. 1193–217.
- [44] Y. YAO, J. CHOI, AND I. PARKER, *Quantal puffs of intracellular Ca2+ evoked by inositol trisphosphate in Xenopus oocytes.*, The Journal of physiology, 482 (1995), pp. 533–553.